



**Forward electrohydrodynamic ink-jet printing of optical microlenses on microfluidic devices.**

Journal:	<i>Lab on a Chip</i>
Manuscript ID	LC-ART-11-2015-001386
Article Type:	Paper
Date Submitted by the Author:	11-Nov-2015
Complete List of Authors:	Vespini, Veronica; Istituto di Scienze Applicate e Sistemi Intelligenti Coppola, Sara; Istituto di Scienze Applicate e Sistemi Intelligenti Todino, Michele; b. Institute for Microelectronics and Microsystems Paturzo, Melania; Istituto di Scienze Applicate e Sistemi Intelligenti Bianco, Vittorio; Istituto di Scienze Applicate e Sistemi Intelligenti Grilli, Simonetta; Istituto di Scienze applicate e Sistemi Intelligenti.E. Caianiello Ferraro, Pietro; Istituto di Scienze applicate e Sistemi Intelligenti.E. Caianiello



Journal Name

ARTICLE

## Forward electrohydrodynamic ink-jet printing of optical microlenses on microfluidic devices.

V. Vespi<sup>a</sup>, S. Coppola<sup>a</sup>, M. Todino<sup>b</sup>, M. Paturzo<sup>a</sup>, V. Bianco<sup>a</sup>, S. Grilli<sup>a</sup> and P. Ferraro<sup>a\*</sup>

Received 00th January 20xx,  
Accepted 00th January 20xx

DOI: 10.1039/x0xx00000x

www.rsc.org/

We report a novel method for direct printing of viscous polymers based on pyro-electrohydrodynamic repulsion system, capable to overcome limitations on the material type, geometry and thickness of the receiving substrate. In fact, the results demonstrate that high viscous polymers can be easily manipulated for optical functionalizing of lab-on-chip devices through demonstration of direct printing of polymer microlenses onto microfluidic chip and optical fibre's termination. The present system has great potential for applications from biomolecules to nano-electronics. Moreover, in order to prove the effectiveness of the system, the optical performance of such microlenses has been characterized by testing their imaging capabilities when the fibroblast cells were let flow inside the microfluidic channel, showing one of their possible applications on-board a LoC platform.

### Introduction:

Nano dispensing of liquids and direct printing methods are becoming the prominent nano-fabrication tools in multiple fields of application [1-4]. Among the various ink-jet printing approaches the most promising techniques appear to be the electrohydrodynamic (EHD) based techniques. The EHD systems have proved challenging spatial resolution down to nanoscale [1], printing of high ordered geometrical patterns [5], capability of dispensing biological ink as DNA and protein array [3,6], single cells printing [7] and direct printing of nanoparticles [8]. Diverse materials with wider range of properties are needed in this process so that the flexibility of the apparatus becomes an essential parameter regarding not only the kind of material processed but also the target substrate used as collector [9-11]. It is currently possible to design and create arbitrary patterns using two main classes of materials, rigid materials, especially metals and semiconductors, or organic molecules [12-14]. However many difficulties still arise in the deposition with high resolution of a third material class, liquids, polymers and hydrogels. During the years, various techniques and methods have been developed for manipulating polymers and dispensing droplets such as ink-jet printing, piezoelectric print heads, EHD jetting and nanoscale EHD

ink-jet printing in combination with the self-assembly of colloidal inks [15-18]. This growing interest is deeply explained considering that liquid inks have been also exploited as universal ink-carriers for functional or biological materials [19]. In fact, the controlled deposition of liquid volumes could expand novel applications such as cell-material interfaces, multi-plexed nano-arrays for high throughput screening of biomolecular interactions and localized delivery of reagents in addition to their well-established use for the fabrication of electronic devices [20-22]. Recently the EHD approach has introduced interesting benefits, the print head can make a range of droplets size from several  $\mu\text{m}$  to hundreds of nm and furthermore highly viscous liquids can be processed preserving the ink properties [23-26]. All EHD configurations for inkjet printing include a counter electrode and a nozzle where droplets are formed applying a high voltage. In fact, the electrostatic field applied draws the meniscus of the liquid into a sharp cone, and charged liquid droplets are attracted by counter electrode the ejected from the nozzle when the electrostatic forces exceed those of surface tension [27]. Unfortunately, for achieving high accuracy in the classical EHD ink-jet apparatus the liquid is not viscous and the distance between the electrode and the counter electrode has to be very small, often down to only hundreds of micrometers [28]. For this reason the set-up often does not allow the insertion of thick substrate between the nozzle and the electrode. This is a severe constrain since on-demand printing cannot be realized on real-device that usually have even millimetre size thickness such as microfluidic chips, or electronic devices. The EHD tip streaming studied by Basaran revealed a printing modality

<sup>a</sup> Institute of Applied Sciences and Intelligent System (CNR-ISASI)

<sup>b</sup> Institute for Microelectronics and Microsystems (CNR-IMM)

\* Corresponding author: Pietro Ferraro

Electronic Supplementary Information (ESI) available: [details of any supplementary information available should be included here]. See DOI: 10.1039/x0xx00000x

in attractive modality directly from a liquid reservoir keeping out the use of the nozzle [29]. In addition more recently a pyro-EHD approach has been developed overcoming the nozzle limitations starting directly from a liquid drop reservoir lying in front of a pyroelectric crystal extending the range of viscosity of the polymer processed [30-32]. In this configuration the liquid jetting follows the direction toward the pyroelectric substrate similar to the classical EHD system in which the liquid jetting is toward the count-electrode surface but with the difference that, in the pyro approach the liquid is attracted towards the substrate and no more rejected from the nozzle. Nevertheless, both classic EHD and the pyro experimental configuration suffer of the same limitation since the receiving substrate has to be inserted in-between the two electrodes at a well-defined distance. In classical EHD the target is inserted between the nozzle and the counter-electrode plate while, in case of the pyro set-up the target is placed between the liquid drop reservoir and the pyroelectric crystal. Limitations on thickness, material type (conductive, liquid, etc..) and geometric constrain reduce significantly the flexibility of EHD systems. Moreover this geometrical constrain represents a severe limitation in case is requested a dispensing/printing directly on devices ready for use, i.e. to functionalize them, the thickness of such device makes it impossible to apply the EHD methods. At the current stage of technology the laser-induced forward transfer (LIFT) [33] technique could be used to overcome these limitations but the LIFT procedure is still very complex. The experimental set-up is quite complicated and requires a laser, a mask to select part of the beam and a camera for imaging the laser spot and control in real time the coaxiality [34] without reaching the printing resolution of the EHD. Here we demonstrate a novel pyro-EHD configuration for printing and transferring liquid shots and

pixels with defined dimensions achieving high resolution even at long distance. The transfer process proposed is triggered by a temperature gradient introducing an oversimplification of the pyro-inkjet printing apparatus and working in repulsive way. In fact, in the set-up proposed the dispenser works in a contact-free modality and is probably very close to the industrial demand being independent to the kind of receiving substrate used and material dispensed. In Fig.1 are shown the schematic set-ups of the classic EHD, EHD tip- streaming, classic pyro-EHD and our forward pyro-EHD apparatus at the aim to visualize the different geometric setup. We show that the thickness's limit of the receiving substrate was removed completely by forward Pyro-EHD systems, overcoming an issue never considered before "the critical parameter for ink printability directly on several devices". The pyro-electric field was activated by a temperature gradient onto a ferroelectric crystal triggers the high resolution printing on demand of very small liquid volumes achieving challenging results even if in case of high-viscous polymer inks. Practical demonstrations in direct printing of poly (methyl methacrylate) (PMMA), poly (lactic-co-glycolic acid) (PLGA), silver-ink are reported. Polymer optical micro-lenses made of polydimethylsiloxane (PDMS) are printed on microdevices for validating the approach in handling high-viscous polymers for practical applications. In particular, we show versatile printing of polymer optical elements directly onto the top of microfluidic chips or optical fiber termination. The optical characteristics, aberrations and focusing properties of such structures are evaluated indicating the feasibility and reproducibility of the forward printing. Moreover we report also on a configuration that allows multi-jets high-resolution printing in the forward modality proposed here.

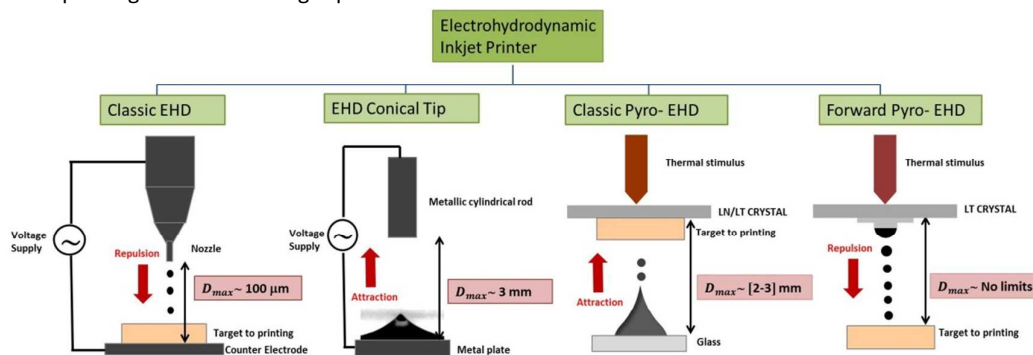


**Figure 1.** EHD printing in a classic configuration, EHD tip streaming from a liquid film, classic pyro-EHD and forward pyro-EHD printing, respectively.

## Experimental setup:

**Fig. 2(a)** shows the outline of the experimental apparatus used in the current work. The system consisted of a heating system, a moving stage system, and a monitoring system. The heating system comprised a conventional soldering iron to produce a thermal stimulus at one side of the lithium tantalate (LT) crystal. The moving stage system comprised of a high precision linear motor with an X-Y axis (SGSP26-100(XY) SIGMA KOKI CO., LTD.) and a digital motion controller (SIGMA KOKI CO., LTD.). The maximum travel speed was 30 mm/s. The monitoring system consisted of a highly-sensitive and fast camera (uEye, USB 3.0, a resolution of 2048 x 2048 pixels), an optical zoom lens, and a blue LED light source (Thorlabs M470L3, wavelength of 470 nm and beam power of about 650 mW), it was used to monitor the cone-jet mode and jetting status, providing a side view of the jetting system. Recently, we developed a pyro-EHD printing system free from nozzles and electrodes based on the use of surface charges generated spontaneously onto pyroelectric crystals [30]. In our previous work the key challenge consisted in optimizing the droplet-to-LT crystal distance to improve the printing of a functional material onto the receiving substrate, that has to be placed in-between the liquid drop reservoir and the pyroelectric crystal. In the previous set-up the restrictions on the distance represents a severe limitation on thicknesses and geometric constrain of the receiving substrate. Instead, in the novel configuration proposed the active control on the distance is not a necessary requirement for a reproducible printing process in fact, the receiving substrate is simply placed in front of the drop reservoir and of the crystal (**Fig. 2(a)**) allowing a direct printing on devices ready for use. A liquid drop is deposited on a PDMS pillar base previously realized on standard glass coverslip to improve the uniformity of the base drops. A wafer of LT (z-cut, 0.5 mm thick) was mounted over the coverslip upon which the drop is supported and was heated locally in correspondence of the base droplet thus allowing the generation of pyroelectric surface charges on the crystal. The liquid droplet starts to deform under the action of the sufficiently strong electric field and releases from conical tip structures a direct-writing of micro-droplets onto a moving substrate. A typical sequence of images placed in **Fig. 2(b)** (more visible in the **Supplementary Movie 1**) illustrates the pyro-EHD printing system under a non-conventional configuration as described previously. The liquid droplet with a little volume on substrates always presents the spherical cap shape due to the surface tension. In order to change the droplet morphology, new force must be introduced to overcome the surface tension. In EHD, the electrostatic force is generated and acts in droplet, when an electric field is applied around the droplet.

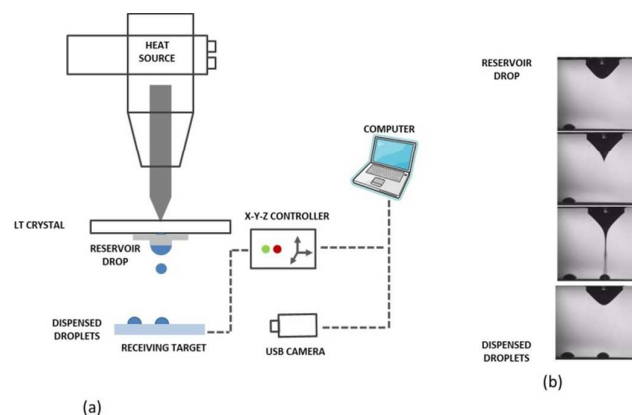


**Figure 2.** (a) Schematic view of the experimental set-up of the pyro-EHD printing system and (b) side view images of a typical sequence of dispensed droplets.

The electrostatic force,  $F_e$ , can be formulated in terms of the Korteweg-Helmholtz force [35]:

$$F_e = \rho_f E - \frac{1}{2} E^2 \nabla \epsilon + \nabla \left( \frac{1}{2} \rho \frac{\partial \epsilon}{\partial \rho} E^2 \right) \quad (1)$$

Where  $\rho_f$  is the free charge density within the fluids,  $E$  is the electric field strength,  $\epsilon$  is the permittivity and  $\rho$  is the density of the liquid. From equation (1), it can be seen that the electrostatic force comprises three parts. The first term on the right side is Coulomb force, and it presents the force per unit volume on a medium containing free charge. The second and the third term presented dielectric force and electrostrictive force, respectively. In this study, the liquid material is usually polymer, and can be regarded as a perfect dielectric. Therefore, the free charge density can be considered as zero. In addition, the permittivity and density of the polymer can be considered as constant. Thus, the Coulomb force and electrostrictive force can be ignored. Equation (1) can be reduced to:

$$F_e = -\frac{1}{2} E^2 (\epsilon_r - \epsilon_0) \quad (2)$$

where  $\epsilon_r$  and  $\epsilon_0$  refer to permittivity of the liquid polymer and air, respectively. It can be observed that the electrostatic force is proportional to the electrical field strength at the local interface. The electric field in equation 2 is due to the pyro-electric effect that is activated through the action of the heating source onto lithium tantalate

plate, any temperature variation causes the generation of free surface charges and resulting high electric fields that are utilized for EHD ink-jet printing [36,37].

### Experimental results:

In this work we patterned a series of polymer dots and lines using a non-conventional EHD jet printing system and measured their sizes with an optical microscope, the patterned drops were uniformly spaced, each drop corresponding to one single release after Taylor's cone formation. Anyway, the desired pattern sizes are realized through repeated printing experiments with various materials (PDMS, PLGA, PMMA and nano-metal ink), operating conditions (without external voltage, no droplet-to-plate distance and nozzle-free), and several substrates. Different behaviour of the meniscus and jetting observed by changing the materials analyzed through a speed camera is shown in Fig. 3(a). In addition, in our experiments different materials for generation of droplets with different properties were tested, among them, the viscosity of the polymer is a more important factor to determine the stable and reproducible droplets, as shown in Fig. 3(b).

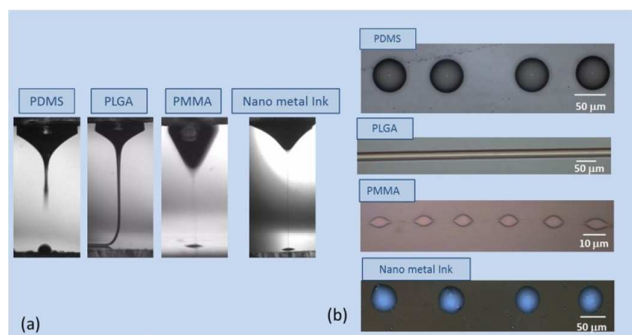


**Figure 3.** (a) Meniscus shapes after application of thermal stimulus on pyroelectric crystal, (b) PDMS, PLGA, PMMA and Nanometal Ink micro-droplets and micro-lines were realized as an alternative to conventional EHD configurations.

In alternate configuration the pyro-EHD field is also able to induce the surface film instability leading to the multiple jetting operation as shown in Fig. 4(a), here we adopt the same instability mechanism for activating an EHD polymeric-multi jets process as described in our previous work [38]. The system proposed here represents the conjugation of the alternative-dispenser with the EHD film instability giving rise to an unconventional multiple dispenser for high viscous polymers, like PDMS where nozzles cannot be adopted. The multi-printing process in modality forward is viewable also in the **Supplementary Movie 2** where the typical jets are captured with a good degree of uniformity. A wide range of materials, can be

printed using this approach, with resolutions extending to the micrometer range. Actually, we have demonstrated the fabrication of ordered patterns with this novel EHD ink-jet approach by the advantages of being electrode-less, nozzle-less and not having the limitations of substrate thicknesses. This technique is flexible and efficient for controllable patterning, constructing a text patterns with a liquid material, as shown in Fig. 4(b). The average dots diameter is between 10- 40 μm, and the uniformity in the sizes is shown in the inset.

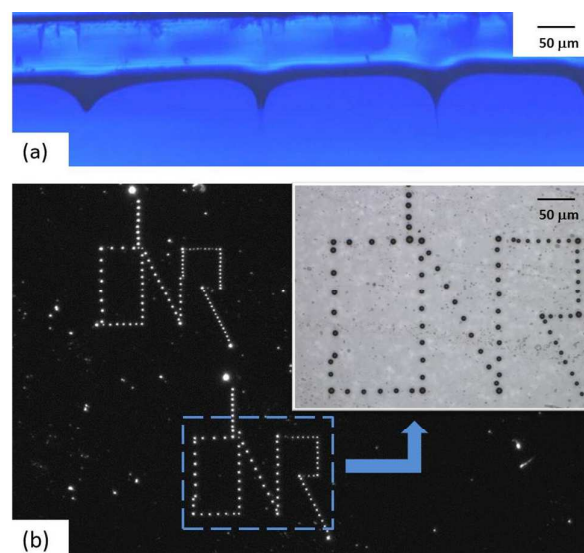


**Figure 4.** (a) Alternative EHD polymeric multi-jets dispenser, (b) Optical microscope image of a dots-matrix constructed a text pattern and inset is a detailed view of the dots matrix, the letters printed with dot diameters of 10-40μm demonstrating their high homogeneity.

**Fig. 5(a)** reports the experimental evaluation of the average volumes of the test materials used in this work in function of their viscosity. It is also shown there are no limits for the forward EHD printing, in fact the corresponding volume of the single dispensed dot is included in a range of  $0,54 \leq V \leq 1,50$  nL even by using high- viscosity liquid. In order to evaluate the uniformity of the dots patterned by the EHD jet printing, first we fabricated a dots matrix by forward printing on the substrate and we have noted that the size of the dot array could be expanded to the larger area. In **Fig. 5(b)** is presented the probability density function of the gaussian function about the values of the diameter of drops, statistically we measured 70 dots which were chosen randomly from the dots array, the average of the dot diameter was 28,55 μm and its standard deviation was 4,19 μm. Furthermore, from these results we noted that there was not a significant variation in the diameter of the dots printed by forward EHD jet printing. In **Fig. 5(c)** is shown the probability density function where was not a

significant variation in the diameter, the mean value is  $31.27 \mu\text{m}$  and standard deviation is  $0.42 \mu\text{m}$ .

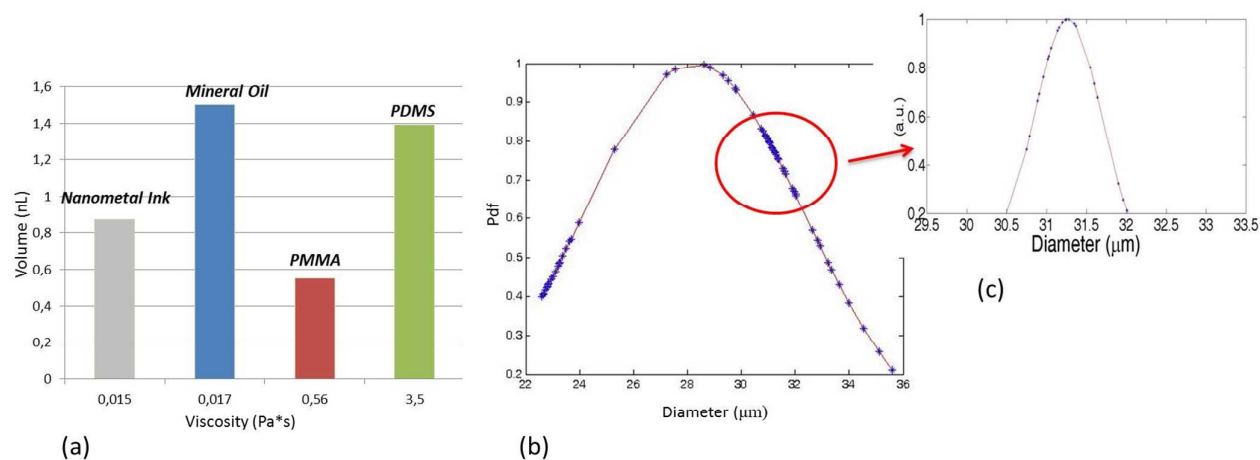


**Figure 5.** (a) Corresponding average volume of the printed dots in relation to their viscosity, (b) Standard deviation on dots diameter randomly chosen from the dots matrix printed, (c) probability density function of higher density of dots printed.

### Direct printing of PDMS microlens on devices:

In our forward configuration for pyro-EHD liquid dispensing is shown that exceeds the limits in direct inkjet printing modality, in fact we have the possibility of dispensing picodrops of liquid material directly on an optical fibre, as shown in **Fig. 6** (see also the **Supplementary Movie 3**). The obtained results show that the novel method proposed is very strong to overcome the limitations on thicknesses, on type materials (liquid, conductive, polymeric) and on geometric constraints reducing significantly the flexibility of the EHD systems. The complexity of accurate positioning and aligning of optical fibre and droplet printing is critical and has advantages such as high-resolution and wide-ranging ink selectivity compared to conventional ink jet printing methods. In fact, it can print droplets as small as a few hundred nanometers.



**Figure 6.** Forward EHD jet printing of a few pico-droplets on aligned optical fibre.

Additionally, the direct writing of the PDMS microlenses onto a conventional microfluidic channel (PMMA material, ChipShop GmbH) as shown in **Fig. 7** opens the way to a new technology for develop and manufacture “lab-on-a-chip” systems mainly in polymers usable in many application fields including microfluidics, chemistry, biology, and diagnostics. In fact, the fabricated microlenses are integrated on microfluidic devices that feature a very flexible design of microchannels, good chemical compatibility and optical properties. The material used for this process is PDMS thanks to high adhesion, curing rapidly and excellent optical performance is preferred for the fabrication of microlenses. **Fig. 7(a)** shows a schematic standard microfluidic chip with simple straight channels on which microlenses have been printed using our EHD ink-jet technique and a complete image of the PDMS microlenses was obtained using a camera as appears in **Fig. 7(c)**. A pattern of microlenses with various shapes was formed through the translation of the chip using a computer-controlled motorized XY stage, after the deposition of the polymer drops they were baked at  $80^\circ \text{C}$  for 30 min. In order to control the geometrical properties such as the diameter and height of the ink-jet printed microlens, a surface treatment was performed using Fluorolink S10 (Solvay Solexis) on a microfluidic chip as shown in **Fig. 7(b)**, representing a contact angle of  $\theta_c \sim 40^\circ$  between the sessile droplet and solid surface. A thin fluorinated layer is created by Fluorolink S10 onto the surface of the channel to reduce the surface energy, coefficient of friction and to enhance oil-water repellency, this thin protective film shows also low refractive index, solvent and abrasion

resistance and antireflection properties. The substrates are previously treated in a low pressure O<sub>2</sub> plasma system (Femto System, Diener Electronic GmbH & Co. KG, Ebhausen, Germany) for micro-cleaning and to activate their surfaces – after the pre-treatment 0.2% wt Fluorolink S10 is diluted in 98.8 % wt isopropyl alcohol, then 0.8% wt water is added, and at the end 0.2% wt acetic acid to start the catalysis. Then, after waiting 30 min. in order to allow the hydrolysis of the siloxane groups, the product is applied by dipping. Subsequently, the fluorinated channels were placed onto a hot plate at T= 80°C for 35 min. for curing the material. The use of microlenses integrated on the microfluidic channel allows the development of fast, portable, and easy-to-use systems with a high level of functional integration. The images in **Figs. 7(d) and 7(e)** were acquired under the optical microscope corresponding to microlenses on the microfluidic chip and to focusing the USAF resolution target through the polymeric microlens, respectively. The focusing capability of the microlens is clearly visible, indeed the PDMS is a highly transparent material with stable optical properties and thus the polymer microlens can present the image with a good quality.

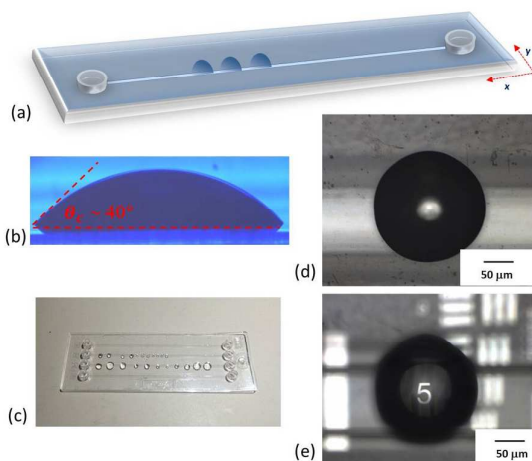


**Figure 7.** (a) Schematic drawing of the one-channel through-hole chip. (b) Cross section view of polymer  $\mu\text{m}$ -lens on a surface treatment using Fluorolink S10 providing a hydrophobic condition. (c) The representative image of the a thin fluorinated layer onto microfluidic chip with printed and cured lenses formed with different diameters of 150-1500  $\mu\text{m}$ . (d) Optical microscope images of the polymer microlens on microfluidic chip. (e) The polymeric microlens was positioned over the USAF target and observed under the optical microscope.

### Interferometric characterization:

An interferometric characterization based on Digital Holography (DH) microscopy [39-42] was carried out in order to evaluate the optical aberrations of the microlenses and their focusing properties. The optical set-up is a classical Mach-Zehnder interferometer in transmission configuration, as sketched and described in detail in the Supporting Information section (**Fig. S1(a)**). The object beam is directed toward the object, namely the microfluidic chip where a sample micro-lens is deposited, and then recombines to the reference in the acquisition plane in order to produce an interference pattern, i.e. the digital hologram shown in **Fig. S1(b)**. Once the hologram is recorded, numerical propagation provides the object complex field in whatever plane along the optical axis,  $z$ , from which the intensity and the phase distributions of the optical wavefield transmitted by the sample can be extracted [39, 41]. A double exposure method was adopted to compensate for the aberrations of the optics in the set-up, as well as the phase delay introduced due to the passage of the object beam through the chip. Hence, the recovered phase-contrast map directly yields information about the lens optical behavior.

A 2D fitting was applied to the recovered phase map, using a Zernike polynomial expansion [43] to model and study the optical aberrations produced by the lens [39, 42, 43]. To assure the best fitting results, the hologram plane was chosen in order to obtain a proper sampling of the object information on the whole lens area. Thus, the optical aberrations were estimated in the hologram plane, far  $d=17,3\text{cm}$  from the lens exit pupil. As a fitting quality index, we computed the Mean Square Error (MSE) between the measured and the calculated phase distribution, normalized with respect to the maximum value of the measured phase map. When  $P_{\text{max}}=10$  terms were adopted to synthesize the Zernike function, a  $\text{MSE}=0.07\%$  was found, assuring a very accurate reconstruction quality. The first 10 orders of the linear combination of Zernike polynomials (i.e. the Zernike function) are shown in **Fig. 8**, along with the corresponding coefficients,  $a_p$ , representing the weight of each aberration term. From the bar diagram of **Fig. 8** it is apparent that, except for the constant offset ( $P=1$ ), the main contribution to the development of the Zernike function is a defocus term ( $P=5$ ). This is an expected result due to the spherical shape of the lens. Moreover, a tilt along the  $y$  axis ( $P=3$ ) is present, as well as a coma aberration along the  $x$  axis ( $P=8$ ). The other terms give a negligible contribution.

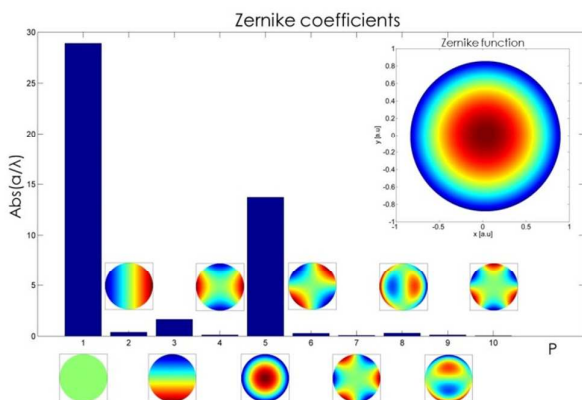


**Figure 8.** Normalized Zernike coefficients derived from the lens phase-contrast map. For each order  $P$ , the corresponding Zernike polynomial is shown.

The distributions of the main aberration orders are reported in **Fig. 9**, while the coefficient values for each aberration term are listed in **Table S1** in the **Supporting Information Section**. If compared to the expected spherical contribution ( $P=5$ ), the aberration spatial distributions depicted in **Fig. 9** show shorter dynamics. Hence, they play a minor role in determining the optical behavior of the micro-lens. In order to estimate the lens focal length, we adopted two different strategies, whose results are in good agreement. As previously discussed, DH allows to numerically perform a  $z$ -scanning in order to reconstruct the complex object wavefield in a convenient plane. Thus, it is simple to measure the focal length as the distance between the lens focus plane and its exit pupil. On the other hand, a geometrical approach can be followed. Indeed, the radius of curvature,  $R$ , can be measured from the phase-contrast map extracted in the plane corresponding to the lens exit pupil. Hence, we estimated the focal length as  $\hat{f} = R/(n-1) = 4,3\text{mm}$ , where  $n=1,46$  is the lens refractive index.

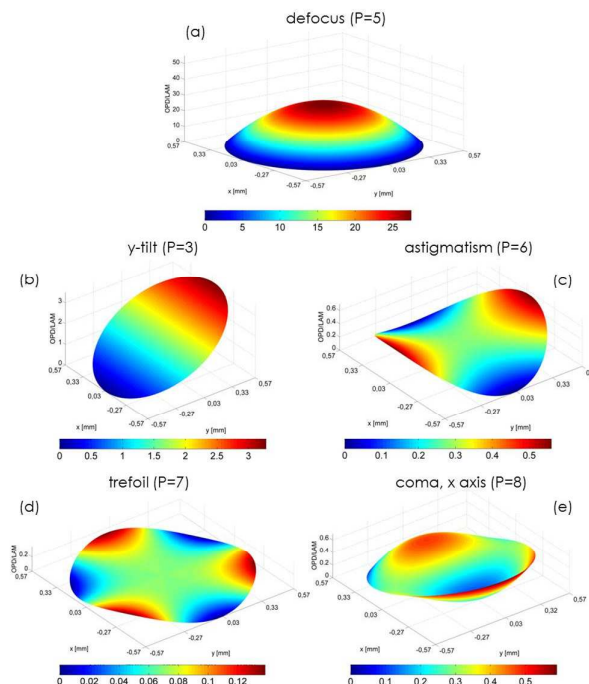


**Figure 9.** Spatial distribution of the main Zernike polynomials. (a) Spherical factor. (b) Tilt along the  $y$ -axis. (c) Astigmatism. (d) Coma aberration,  $x$ -axis.

### Test of the PDMS lens on microfluidic channel:

A lot of international articles have been recently produced investigating the novel concept of 'lab-on-a-chip', which corresponds to the integration of all the components directly on a chip to perform a complete biochemical analysis, including a detection step [44]. Once the optical characterization of the polymeric micro-lenses was carried out, their imaging capabilities were tested showing one of their possible applications onboard a LoC platform. At this scope, fibroblast cells were let flow inside the microfluidic channel where the lenses were directly deposited and imaged through an optical microscope. **Figures 10(a),(b)** show the images of the cells inside and outside the lens area. In particular, these are clearly imaged in focus only when they flow behind the lens, while these are out-of-focus in all the other portions of the channel. In **Figure 10(a)** it is also possible to notice the magnifying action operated by the lens, as the channel itself appears to be enlarged. In order to make more apparent this capability, the DH set-up described in the **Supporting Information Section (Fig. S1)** was employed to capture holograms of a test resolution target placed behind the chip in the sample plane. In particular, two out-of-focus holograms were recorded while shifting the target with respect to the lens, and numerical hologram propagation provided the

refocused image of the object. In this way, it has been possible to proof the lens magnification. Indeed, the smallest target segments in the red box of **Fig. 10(c)** are not visible at all, while these get resolved when observed through the lens (see the area in the red box in **Fig. 10(d)**). Thanks to the possibility to directly write lenses on-board chip, it becomes possible to dramatically increase the information throughput from samples flowing along microfluidic paths, as different magnifications could be provided after a single passage of the specimens through the channel.

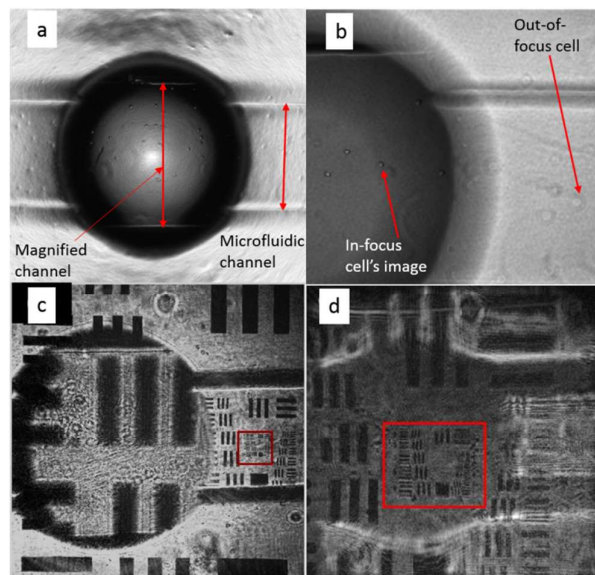


**Figure 10.** Microlenses were directly deposited onboard chip. (a,b) Fibroblast cells flowing inside a microfluidic channel are imaged in focus through the lens, while out-of-focus images of the cells are obtainable outside the lens area. (c-d) A test resolution target was put behind the chip for test purposes. Two DH reconstructions show the magnification action operated by the lens. The microfluidic channel is clearly magnified as well as the target section indicated by the red box. The smallest target elements are not visible at all outside the lens (c), but these get resolved inside the lens area (d).

### Summary:

In conclusion, we have successfully demonstrated an alternative EHD jet printing with various inks to generate polymer optical elements directly onto the top of microfluidic chips and on optical fiber. We take advantage of the ability to create stable jetting from using a forward EHD technique, thus overcoming the limitations that usually occur in all previous EHD based ink-jet printing systems in which the substrate must be sandwiched between the electrodes. Problems connected to the size, shape and nature of the materials of the substrate can be neglected

since the EHD is able to deliver at nanoscale volume drops forward the substrate without electrodes and nozzle maintaining very high-resolution and uniformity in the printing action. Moreover, the experimental demonstration of in focus imaging through the lenses of fibroblast cells flowing inside a microfluidic chip is implemented. This novel approach opens the route for a practical application of direct printing on any device.

### Acknowledgements:

This work was supported by the MAAT project PON02\_00563\_3316357.

### References:

1. J.U. Park, J.H. Lee, U. Paik, Y. Lu and J.A. Rogers, *Nanoletters*, 2008, 8, 4210-4216.
2. F. Loffredo, A. De Girolamo Del Mauro, G. Burrasca et al. *Sens. and Act. B- Chem.*, 2009, 143, 1, 421-429.
3. B.H. Kim, M.S. Onses, J.B. Lim, B. Jong et al., 2015, 15, 2, 969-973.
4. H. Yu-Ching, H. Fan-Hsuan, C. Hou-Chin, et al., *Organic Electronics*, 2013, 14, 11, 2809-2817.
5. L. Persano, A. Camposeo and D. Pisignano, *Journal of Mater. Chem.*, 2013, 1, 46, 7663-7680.
6. K. Shigeta, Y. He, E. Sutanto, et al., *Anal. Chem.*, 2012, 84, 22, 10012-10018.
7. K. Ju-Han, L. Dae-Young, H. Jungho et al., 2009, 7, 6, 829-839.
8. L. Jiantong, U. Tomas, C. Ana Lopez, et al., *Journal of Appl. Phys.*, 2011, 109, 8, 084915.
9. I. Mustaffa, O. Takayuki, N. Hiroyuki, et al. *JSME Intern. Journal, Series C*, 2006, 49, 2 353-360.
10. S. Khalil, J. Nam, and W. Sun, *Rapid Prot. Journ.*, 2005, 11, 1, 9-17.
11. J.F. Mei, M.R. Lovell, and M.H. Mickle, *IEEE Trans. on Electr. Pack. Manuf.*, 2005, 28, 3, 265-273.
12. J.L. Wilbur, A. Kumar, E. Kim and G. Whitesides, *Adv. Mater.*, 1994, 6, 600-604.
13. B.D. Gates, Q. Xu, M. Stewart, D. Ryan, C.G. Willson and G.M. Whitesides, *Chem Rev.* 105, 2005, 4, 1171-1196.
14. R.D. Piner, J. Zhu, F. Xu, S. Hong and C.A. Mirkin, *Science* 283, 1999, 5402, 661-663.
15. G. Riboux, A.G. Marin, I.G. Loscertales and A. Barrero, *J. Fluid Mech.*, 2011, 671, 226-253.
16. D.Y. Yang, B. Lu, Y. Zhao, X.Y. Jiang, *Adv. Mater.*, 2007, 19, 3702.
17. Z.P. Zhou, C.L. Lai, L.F. Zhang, Y. Qian, H.Q. Hou, D.H. Reneker and H.H. Fong, *Polymer*, 2009, 50, 2999-3006.
18. P. Galliker, J. Schneider, H. Eghlidi, S. Kress, V. Sandoghdar and D. Poulikakos, *Nat. Comm.*, 2012, 3, 890.
19. A.J. Senesi, D.I. Rozkiewicz, D.N. Reinhoudt, C.A. Mirkin, *ACS Nano.*, 2009, 3, 8, 2394-2402.
20. S.D. Arrowood, A.W. Yaniv, *American Journal of Health-System Pharmacy*, 2015, 72, 1, 1-21.

21. S.R. Caliari, E.A. Gonnerman, W.K. Grier, D.W. Weisgerber, J.M. Banks, A.J. Alsop, J.S. Lee, R.C. Bailey and B.A.C. Harley, *Advanced Healthcare Materials*, 2015, 4, 1, 58-64.

22. P. Viswanathan, M.G. Ondeck, S. Chirasatitsin, K. Ngamkham, G.C. Reilly, A.J. Engler and G. Battaglia, *Biomaterials*, 2015, 52, 140-147.

23. Y. Duan, Y. Huang, Z. Yin, N. Bu and W. Dong, *Non-Wrinkled, Highly Stretchable Piezoelectric Devices by Electrohydrodynamic Direct-Writing*, *Nanoscale*, 2014, 6, 6, 3289-3295.

24. C. Wei, H. Qin, N.A. Ramírez-Iglesias, C.P. Chiu, Y.S. Lee and J. Dong, *High-Resolution Ac-Pulse Modulated Electrohydrodynamic Jet Printing on Highly Insulating Substrates*, *J. Micromech. Microeng.*, 2014, 24, 4.

25. M. Kuang, L. Wang and Y. Song, *Advanced Materials*, 2014, 26, 6950-6958.

26. B. Bao, J. Jiang, F. Li, P. Zhang, S. Chen, Q. Yang, S. Wang, B. Su, L. Jiang and Y. Song, *Advanced Functional Materials*, 2015, 25, 22, 3286-3294.

27. J. Park, B. Kim, S.Y. Kim and J. Hwang, *Applied Physics A-Materials Science & Processing*, 2014, 117, 4, 2225-2234.

28. J. Park, M. Hardy, S.J. Kang, et al., *Nat. Mat.*, 2007, 6, 10, 782-789.

29. R.T. Collins, J. Jones, M.T. Harris and O.A. Basaran, *Nat. Phys.*, 2008, 4, 2, 149-154.

30. P. Ferraro, S. Coppola, S. Grilli, et al. *Nat. Nanotech.*, 2010, 5, 6, 429-435.

31. S. Coppola, V. Vespini, G. Nasti, et al. *Chem. of Mat.*, 2014, 26, 11, 3357-3360.

32. I.A. Grimaldi, S. Coppola, F. Loffredo, et al. *Optics Letters*, 2012, 37, 13, 2460-2462.

33. A.K. Diallo, L. Rapp, P. Cremillieu, R. Mazurczyk, F. Serein-Spirau, J.P. Lère-Porte, P. Delaporte, A.P. Alloncle, C. Videlot-Ackermann and C. Constantinescu, *Applied Surface Science*, 2015, 336, 11-15.

34. C. Florian, F. Caballero-Lucas, J.M. Fernández-Pradas, R. Artigas, S. Ogier, D. Karnakis and P. Serra, *Applied Surface Science*, 2015, 336, 304-308.

35. P.A. Kralchevsky, K.D. Danov and N.D. Denkov, K.S. Birdi, Ed., *CRC Press*, Boca Raton, FL, 1997, 341.

36. E.M. Bourim, C-W Moon, S-W Lee, I.K. Yoo, *Physical B* 2006, 383, 171.

37. G. Rosenman, D. Shur, Y.E. Krasik, A. Dunaevsky *J. Appl. Phys.* 2000, 88, 6109.

38. S. Coppola, V. Vespini, S. Grilli, et al., *Lab on a chip*, 2011, 11, 19, 3294-3298.

39. P. Marquet, C. Depeursinge and P.J. Magistretti, *Neurophoton.*, 2014, 1, 2, 020901.

40. F. Merola, P. Memmolo, L. Miccio, V. Bianco, M. Paturzo and P. Ferraro, *IEEE*, 2015, 103, 2, 192-204.

41. V. Bianco, M. Paturzo, V. Marchesano, I. Gallotta, E. Di Schiavi and P. Ferraro, 2015, *Lab Chip* 15, 9, 2117-2124.

42. L. Miccio, A. Finizio, S. Grilli, V. Vespini, M. Paturzo, S. De Nicola and P. Ferraro, *Opt. Exp.*, 2009, 17, 4, 2487-2499.

43. D.R. Iskander, M.R. Morelande, M.J. Collins and B. Davis, *IEEE Trans. Biomed. Eng.*, 2002, 49, 4, 320-328.

44. S. Camou, H. Fujita and T. Fujii *Lab Chip*, 2003, 3, 40-45